JOURNAL OF MATERIALS SCIENCE **39** (2004) 2011–2015

Numerical study on directional solidification of AlSi alloys with rotating magnetic fields under microgravity conditions

M. HAINKE, J. FRIEDRICH, G. MÜLLER
Crystal Growth Laboratory, Fraunhofer Institute IISB, Erlangen, Germany
E-mail: marc.hainke@iisb.fraunhofer.de

A global thermal model of the ARTEX facility, developed with the modeling tool CrysVUn, is presented. The model is validated with experimental data obtained under microgravity conditions during the TEXUS39 mission. Numerical studies are then reported, in which the effects of a rotating magnetic field are investigated during directional solidification of binary AlSi7 alloys. It appears that beyond a certain magnetic field strength a macrosegregation effect is resulting, leading to the development of a liquid channel inside the mushy zone.

Nomenclature

b	body forces (N/m^3)
B	magnetic field strength (T)
C	concentration (wt.pct.)
f	frequency (1/s)
G	temperature gradient (K/m)
H	height (m)
K	mushy zone permeability (m^2)
m	liquidus line slope (K/wt.pct.)
p	number of pole pairs; pressure (Pa)
R	radius (m)
T	temperature (K)
u	flow velocity (m/s)
v_G	growth velocity (m/s)
X	phase function
X^*	depth of mushy zone concerned with flow (m)
δ	extension (m)
ε	volume fraction
ϕ	physical quantity
λ	eutectic spacing (m); primary dendritic arm spacing (m)
μ	magnetic permeability (Vs/Am); dynamic viscosity (kg/ms)
ν	kinematic viscosity (m^2/s)
ρ	density (kg/m^3)
σ	electrical conductivity (S/m)
ϖ	rotating frequency (1/s)
Δ	increment
Γ	convective parameter
Ω	volume element

Subscripts

b	buoyancy force
E	eutectic
k	phase k, either solid s or liquid l
L	Lorentz force
m	magnetic field
MZ	mushy zone
r	radial flow velocity
z	axial flow velocity
0	representative element or initial value
φ	azimuthal flow velocity

1. Introduction

Many alloys are solidifying with a dendritic columnar structure. This region, where solid and liquid phase are co-existent within a certain temperature interval is usually called the mushy zone. The mushy zone is a consequence of transport processes, capillarity effects and thermodynamic constraints.

Nowadays the effects of convective heat and mass transport experience enhanced attention [1]. Phenomena on different length scales are influenced by convection. On the scale of a single dendrite, convection may lead to a changed morphology of the dendrites or may even lead to fragmentation. On the scale of the whole sample, convection is mainly responsible for the effect of macrosegregation, i.e., concentration inhomogenities at the scale of the sample.

Time dependent magnetic fields are recently considered as a promising option for systematic investigations on the effects of fluid flow during alloy solidification [2, 3]. Thereby, dependent on the field configuration, different flow patterns are created inside the melt. Within the MICAST[1] project [2, 3] especially rotating magnetic fields (RMFs) are investigated, as these fields will be available in two furnace inserts in the Material

[1]MICAST—Microstructure formation in casting of technical alloys under diffusive and magnetically controlled convective conditions (ESA MAP AO-99-031).

Science Laboratory on the International Space Station ISS [4].

The action of RMFs has been studied numerically in a number of publications, e.g., [5–8]. It is well known, that the use of RMF is an efficient tool for controlling the melt flow and thus can affect the temperature and species distribution [9–11]. Indeed, RMFs are nowadays industrially commonly in use to influence alloy solidification, mainly to create a finely dispersed equiaxed microstructure. Nevertheless, the number of publications with numerical investigations on the resulting macrosegregation during alloy solidification is very limited. This is mostly due to the high computational costs of the pertinent calculations. Recently, segregation effects resulting from traveling magnetic fields during directional solidification are reported in [12, 13]. The effects of RMFs during equiaxed solidification are investigated in [14].

In this work we report about applications of the global modeling tool CrysVUn [15, 16]. A thermal model of the ARTEX facility is presented and validated with experimental data obtained during the TEXUS39 mission. A re-flight of the facility is scheduled for TEXUS41, then equipped with an additional RMF. Therefore, numerical studies are presented in this work, in which the principal effects of the RMFs during directional solidification are analyzed.

2. Global modeling with CrysVUn

CrysVUn [15, 16] contains physical modules for heat transfer by conduction, radiation and convection. Additionally, the possibility of inverse modeling is comprised, which allows to control the temperature in a certain number of points. The finite volume technique in conjunction with unstructured triangular grids is applied for the discretization [17]. The program was originally designed for global simulation of crystal growth experiments, but was recently extended with a model for macrosegregation during alloy solidification. The solidification model is based on the classical volume averaging procedure applied to the conservation equations of heat, mass, momentum and chemical species [18]. Thereby, we have adopted a model originally proposed by Poirier and co-workers [19, 20].

On the macro scale the equations for each phase k (solid s or liquid l) are formulated in terms of averaged quantities for a representative elementary volume Ω_0

$$\langle \phi_\mathrm{k} \rangle = \frac{1}{\Omega_0} \int_{\Omega_0} X_\mathrm{k} \phi_\mathrm{k} \, \mathrm{d}\Omega \tag{1}$$

whereby X_k is a phase function (1 in phase k, 0 elsewhere) and ϕ a physical quantity. The volume fraction of a phase k is defined as

$$\varepsilon_\mathrm{k} = \frac{\Omega_\mathrm{k}}{\Omega_0} \tag{2}$$

The mixture concentration is defined as

$$\langle C_\mathrm{mix} \rangle = \varepsilon_\mathrm{s} \langle C_\mathrm{s} \rangle^\mathrm{s} + \varepsilon_\mathrm{l} \langle C_\mathrm{l} \rangle^\mathrm{l} \tag{3}$$

whereby $\langle C_\mathrm{k} \rangle^\mathrm{k}$ is the average concentration within the solid resp. liquid phase. Changes of the mixture concentration from the initial concentration are mainly due to fluid flow within the two phase region.

The flow within the mushy region is as usual modeled by Darcy's law

$$\langle u \rangle = -\frac{K}{\mu} (\nabla \langle p \rangle + b_\mathrm{L} + b_\mathrm{b}) \tag{4}$$

with the superficial velocity $\langle u \rangle$, the permeability K, the dynamic viscosity μ, the pressure $\langle p \rangle$, and two body forces, the Lorentz force b_L and the buoyancy forces b_b. The permeability of the mushy zone is a function of the liquid volume fraction and the spacing of the dendritic microstructure.

Inside the mushy region, the temperature $\langle T \rangle$ and the concentration in the liquid phase are coupled via the phase diagram

$$\langle T \rangle = T_\mathrm{pure} + m \cdot \langle C_\mathrm{l} \rangle^\mathrm{l} \tag{5}$$

with the melting point of the pure substance T_pure and the liquidus line slope m.

More details on the model can be found in the above cited literature.

3. Directional solidification experiment with a RMF scheduled for TEXUS41

3.1. Validation of the global furnace model

ARTEX (ARtemis on TEXus) is a further development of the ARTEMIS facility [21, 22] and was built for experiments under microgravity conditions onboard TEXUS [23]. The furnace principle is based on the well-established power-down method. The core part of the furnace consists of two heating elements (boron nitride resistance heaters), separated by a highly insulating silica aerogel which acts both, as sample cartridge and adiabatic zone. The solidification process is monitored by optical means through the transparent aerogel crucible. Additional constructive parts are added due to mechanical reasons. The thermal model of ARTEX as implemented in CrysVUn and the mesh as used in the calculations is shown in Fig. 1.

The thermal model was validated with the experimental data obtained during the TEXUS39 mission. Linear temperature profiles were applied in the experiment to obtain a constant solidification for 300 s in a microgravity environment. As can be seen from Fig. 2, the numerical predictions agree nicely to the experimentally determined position of the solidification front. A shift of 20 K was added to the heater temperatures in the simulations, in order to match the initial position of the solidification front. The extension of the mushy region of $\delta_\mathrm{MZ} = 21$ mm is in good agreement with the experimentally observed value.

Numerical studies show that the radiative heat loss through the aerogel crucible is rather small. The Biot number, defined as the ratio of radial and axial heat fluxes is in the order of $Bi = 0.05$. A planar solidification interface is therefore resulting, both in the experiment and simulation.

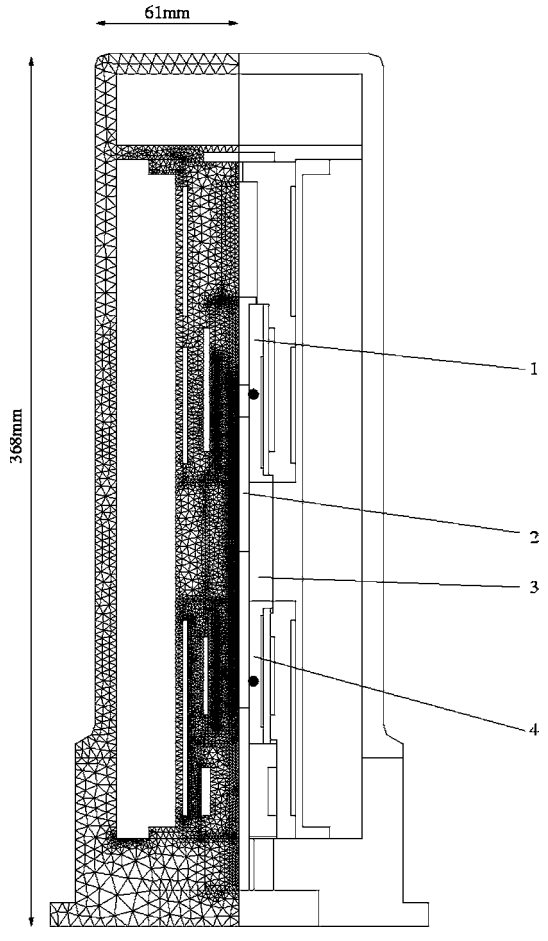

Figure 1 Thermal model of the ARTEX facility as implemented in CrysVUn. The hot zone consists of a top heater (1), the AlSi sample (2), the aerogel crucible (3) and a bottom heater (4).

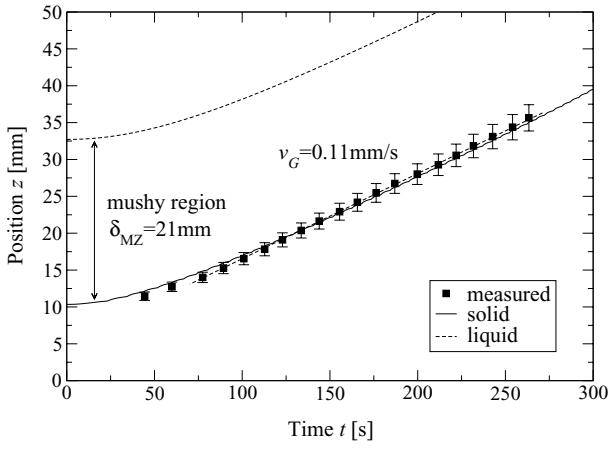

Figure 2 Simulated and measured position of the solidification front for the experiment on TEXUS39.

3.2. Parameter studies on the influence of a RMF during directional solidification

To systematically investigate the effects of a RMF during directional solidification of a binary AlSi7 alloy, numerical studies were performed considering a cylindrical geometry with well defined boundary conditions, as shown in Fig. 3. Temperature profiles are applied at the top and the bottom wall, to achieve a constant solidification from the bottom to the top, with a constant temperature gradient ahead of the mushy zone.

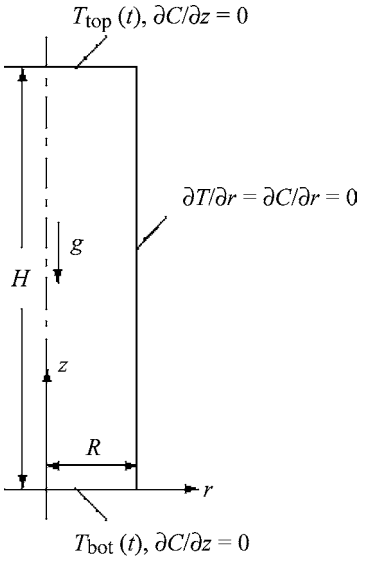

Figure 3 Boundary conditions and geometry as used for the numerical investigations.

The main issues that shall be addressed in the following are:

- What are the typical flow velocities in the bulk liquid due to the RMF?
- Does the bulk flow enter the mushy region and how far?
- How is the shape of the mushy region influenced by the forced flow?

The parameters for the investigations were chosen corresponding to the ARTEX experiment:

- growth velocity $v_G = 0.1$ mm/s
- temperature gradient $G = 4$ K/mm (higher than during the TEXUS39 mission)
- sample radius $R = 4$ mm
- sample height $H = 100$ mm
- magnetic field frequency $f = 50$ Hz
- magnetic field strength $B_0 = 0$–6 mT

The Carman-Kozeny equation [24] is applied for the permeability in the mushy region

$$K = \frac{\lambda_1^2}{180} \frac{\varepsilon_l^3}{(1-\varepsilon_l)^2} \tag{8}$$

whereby the primary arm spacing was set to $\lambda_1 = 310\ \mu$m in the calculations.

The skin depth is estimated as

$$\delta_{\text{skin}} = \sqrt{2/(\mu_m \sigma \varpi)} \approx 3.7 \times 10^{-2}\ \text{m} \gg R \tag{9}$$

whereby μ_m is the magnetic permeability, σ the electrical conductivity and $\varpi = 2\pi f$ the rotating frequency. As can be seen, the magnetic field fully penetrates the sample.

A stationary flow is resulting for the chosen magnetic field parameters. The transition to a time dependent flow is estimated from the critical magnetic Taylor number [25] to occur at a magnetic field strength of $B_0 \approx 8$ mT for the initial aspect ratio.

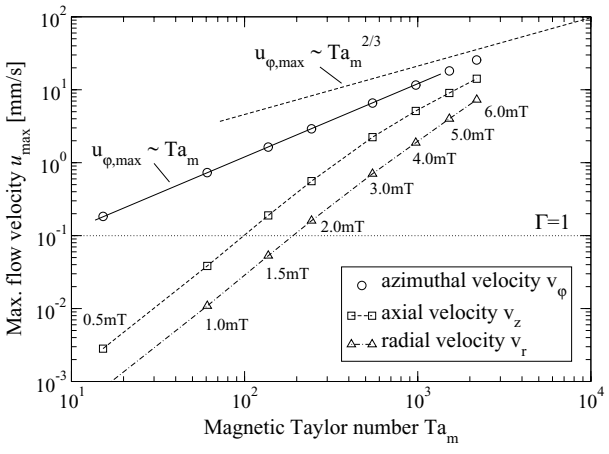

Figure 4 Maximum flow velocities resulting for different magnetic field strengths in the isothermal case.

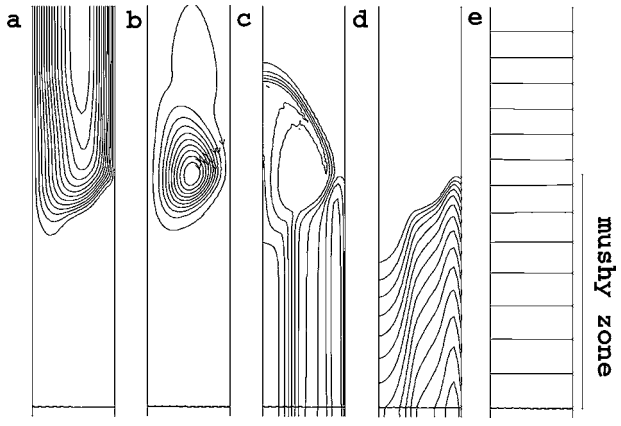

Figure 5 Snapshot after a solidification time of 350 s with $B_0 = 3$ mT. Shown are the isolines of the azimuthal velocity (a), the streamlines (b), the mixture concentration (c), isolines of the liquid fraction (d) and temperature isotherms in steps of 5 K (e). The axis of symmetry is always located on the left side.

Isothermal melt flow calculations have been performed in the beginning, to determine the max. resulting flow velocities, given in Fig. 4. As usual, the magnetic field strength is characterized in terms of the magnetic Taylor number, defined as

$$Ta_\mathrm{m} = \frac{B_0^2 R^4 \sigma \varpi}{2\rho\nu^2 p} \tag{10}$$

whereby ρ is the density of the fluid, ν the kinematic viscosity and p the number of pole pairs ($p = 1$).

As expected the main action of the RMF is a creation of a flow in the azimuthal direction. The max. azimuthal flow velocities follow the theoretical $u_{\varphi,\max} \propto Ta_\mathrm{m}$ relation [26]. Nevertheless, for higher magnetic field strengths, also the secondary flows are strongly increasing, nearly up to the same order of magnitude as the primary flow [27].

In the case of pure diffusive conditions, the extension of the mushy region is approximately

$$\delta_\mathrm{MZ} = \frac{m}{G}\,(C_0 - C_\mathrm{E}) \approx 11 \text{ mm} \tag{11}$$

with the liquidus line slope $m = -6.62$ K/wt.pct, the initial Si concentration $C_0 = 7$ wt.pct and the eutectic concentration of the binary AlSi system $C_\mathrm{E} = 12.6$ wt.pct.

For the considered alloy, the Schmidt number Sc = 332 is much higher, than the Prandtl number Pr = 0.04. This implies that the concentration distribution will be changed at much smaller flow velocities than the temperature field. Therefore, the secondary flows may lead to a macrosegregation effect, and thus lead to a (macroscopic) deformation of the two phase region [28].

Order of magnitude analysis [29–32] gives for the concentration increment

$$\Delta C = \Gamma \frac{G}{m} X^* \tag{12}$$

whereby Γ is a convective parameter, defined as $\Gamma = u_z/v_\mathrm{G}$ and X^* is a characteristic depth concerned with fluid flow. In the case $\Gamma \geq 1$, a pronounced segregation is expected to occur [28].

From the flow velocities given in Fig. 4, this suggests, that the magnetic field strength should be around 2 mT. Nevertheless, it should be noted that this is of course only a rough estimate, as the velocities in the mushy zone are much smaller than the max. values in the bulk liquid.

The fluid flow and the resulting deformation of the two phase region is shown in Fig. 5. Due to the secondary flows, solutal enriched liquid (the liquid concentration is continuously increasing along the liquidus line until the eutectic concentration) is transported out of the mushy region at the axis of the sample. The computed maximum value of the mixture concentration is $\langle C_\mathrm{mix} \rangle = 9.2$ wt.pct. The temperature field is still nearly unchanged. In consequence, a liquid channel is developing at the axis of the sample.

The bulk liquid flow enters the mushy region only at the very top. The max. azimuthal flow velocity is $u_\varphi = 6.6$ mm/s, the max. meridional flow velocity is $u = 2.3$ mm/s.

Axial concentration profiles resulting for different magnetic field strengths after solidification are shown in Fig. 6. For magnetic field strengths smaller than 1 mT no segregation effect is observed. After an initial transient, a constant concentration increment is obtained for

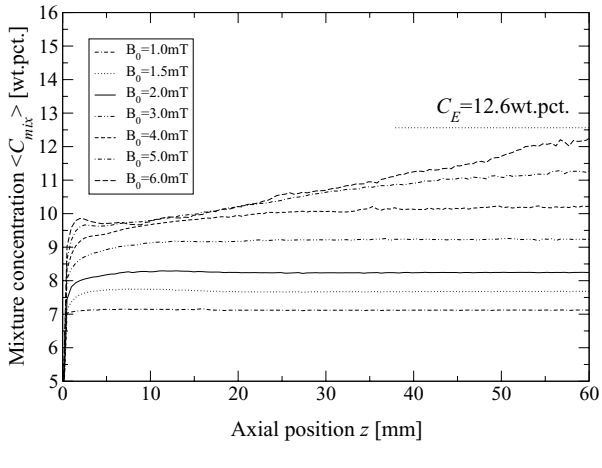

Figure 6 Axial segregation profiles resulting for different magnetic field strengths.

magnetic field strengths up to 3 mT. For higher magnetic field strengths, the concentration is continuously increasing along the axis of the sample. Here, solidification is finally terminated with a pure eutectic reaction, i.e., without mushy region in the center of the sample.

It appears that the mechanism of the RMF on a macroscopic scale is the creation of a segregated channel due to the forced flow within the mushy region. The liquid motion in the liquid zone is primarily due to pressure variations along the solidification front caused by the RMF, which force a liquid flow inside the mushy zone as in a usual porous medium [13]. Secondly, the electromagnetic forces that are acting directly on the liquid phase within the two phase region may contribute to the creation of the interdendritic flow.

Therefore, it can be stated that the RMFs are leading to a macrosegregation effect, even in small scale AlSi samples. The absolute value of the macrosegregation shown in Fig. 6 is dependent on the primary arm spacing. As expected, the segregation is higher for an increased arm spacing. Nevertheless, simulation results (not reported here) show that the dependency on the primary arm spacing is only in the range of a few percentages.

For higher magnetic field strengths fragmentation may occur, leading to a change in the microstructure from columnar to equiaxed.

4. Conclusions

Controlling the melt flow by time-dependent magnetic fields seems to offer the possibility for systematic investigations of the effects of convection on the solidification of metallic alloys. Thereby, due to the complexity of the appearing phenomena, numerical modeling plays an important role in the definition of process parameters and the evaluation of experiments. The conformities between simulation and experiment give trust into the predictive power of modern numerical software tools.

The presented parameter study is used to define the experiment of ARTEX scheduled for TEXUS41. The experimental validation of the presented numerical results is underway.

Acknowledgements

We thank Prof. Dr. L. Ratke and S. Ahrweiler from the Institute for Space Simulation, DLR, for the experimental data.

This work was financially supported by ESA under contract no. 14347/00/NL/SH and by the DLR under contract no. 50WM0042 in the framework of the MICAST research project.

References

1. C. BECKERMANN, *Enc. Mater. Sci. Tech*. (2001) 4733.
2. M. HAINKE, J. FRIEDRICH and G. MÜLLER, MHD Effects in Crystal Growth and Alloy Solidification, in Proc. Int. Sci. Col. Modelling Electromagnetic Processing (2003) p. 73.
3. G. MÜLLER and J. FRIEDRICH, The Influence of Steady and Alternating Magnetic Fields in Crystal Growth and Alloy Solidification: Industrial Importance, Current Industrial R&D Topics, Links to Micro-Gravity research, in Proc. 2nd Europ. Symp. Util. ISS, ESTEC, Noordwijk, ESA SP-433 (1999) p. 309.
4. Material Science Laboratory, http://www.estec.esa.nl/spaceflight/msl.htm, 28/10/2003.
5. P. A. DAVIDSON and J. C. R. HUNT, *J. Fluid Mech.* **185** (1987) 67.
6. P. A. DAVIDSON, *ibid.* **245** (1992) 669.
7. Y. GELFGAT, J. KRUMINS and B. LI, *J. Cryst. Growth* **210** (2000) 788.
8. Y. GELFGAT, Y. KRUMINS and M. ABRICKA, *Mag. Hyd.* **35** (1999) 1.
9. D. DOLD, *J. Cryst. Growth* **231** (2001) 95.
10. J. FRIEDRICH, Y.-S. LEE, B. FISCHER, C. KUPFER, D. VIZMAN and G. MÜLLER, *Phys. Fluids* **11**(4) (1999) 853.
11. B. FISCHER, J. FRIEDRICH, H. WEIMANN and G. MÜLLER, *J. Cryst. Growth* **198/199** (1999) 170.
12. P. J. PRESCOTT and F. P. INCROPERA, *J. Heat Trans.* **117** (1995) 716.
13. G. QUILLET, A. CIOBANAS, P. LEHMANN and Y. FAUTRELLE, Meso-Segregations During Solidification in a Binary Alloy Under the Influence of Convection, in Proc. Int. Sci. Col. Modelling for Electromagnetic Processing (2003) p. 17.
14. J. K. ROPLEKAR and J. A. DANTZIG, *Int. J. Cast. Metals Res.* **14** (2001) 79.
15. M. KURZ, A. PUSZTAI and G. MÜLLER, *J. Cryst. Growth* **198/199** (1999) 101.
16. M. HAINKE, T. JUNG, J. FRIEDRICH, B. FISCHER, M. METZGER and G. MÜLLER, Progress in Ind. Math. ECMI 2000, Springer (2002) p. 218.
17. Y. STRY and M. HAINKE, *Int. J. Num. Meth. Heat & Fluid Flow* **12**(8) (2002) 1009.
18. C. BECKERMANN and C. Y. WANG, *Begell House, Inc.* **3**(6) (1995) 115.
19. D. R. POIRIER, P. J. NANDAPURKAR and S. GANESAN, *Metall. Trans.* B **22** (1991) 889.
20. P. J. NANDAPURKAR, D. R. POIRIER and J. C. HEINRICH, *Numer. Heat Transfer* A **19** (1991) 297.
21. J. ALKEMPER, *et al*., *J. Cryst. Growth* **191** (1998) 252.
22. S. SOUS, Instationäre Erstarrung Eutektischer AlSi-Legierungen, Phd-thesis, Aachen, 2001.
23. S. AHRWEILER, *et al*., ARTEX—Directional solidification of Technical Al-Alloys in ARTEMIS on TEXUS, in Proc. Int. Symp. Microgravity Res. & Appl., Sorrento, Italy, 2000.
24. M. KAVIANY, Principles of Heat Transfer in Porous Media, Springer, 1999.
25. M. HAINKE, J. FRIEDRICH and G. MÜLLER, Numerical study of the Effects of Rotating Magnetic Fields During VGF Growth of 3″GaAs crystals, in Proc. 5th Int. Pamir Conf. (2002) p. V1.
26. R. U. BARZ, *et al*., *J. Cryst. Growth* **180** (1997) 410.
27. P. A. DAVIDSON and F. BOYSAN, *Appl. Sci. Res.* **44** (1987) 241.
28. M. D. DUPOUY and D. CAMEL, *J. Cryst. Growth* **183** (1998) 469.
29. R. MEHRABIAN, M. KEANE and M. C. FLEMINGS, *Met. Trans.* **1** (1970) 1209.
30. P. LEHMANN, *et al*., *J. Cryst. Growth* **183** (1998) 690.
31. M. D. DUPOUY, D. CAMEL and J. J. FAVIER, *Acta Metall.* **37**(4) (1989) 1143.
32. M. D. DUPOUY, B. DREVET and D. CAMEL, *J. Cryst. Growth* **181** (1997) 145.

Received 19 May
and accepted 24 November 2003